Available online at www.sciencedirect.com
SCIENCE DIRECT®
Physics of the Earth and Planetary Interiors 135 (2003) 77–91
PHYSICS OF THE EARTH AND PLANETARY INTERIORS
www.elsevier.com/locate/pepi

High-resolution magnetic field modeling: application to MAGSAT and Ørsted data

Benoit Langlais [a,b,*], Mioara Mandea [a], Pascale Ultré-Guérard [c]

[a] *Institut de Physique du Globe, B.P. 89, 4 Place Jussieu, 75252 Paris cedex 5, France*
[b] *NAS/NRC at NASA/GSFC, code 921, Greenbelt, MD 20771, USA*
[c] *Centre National d'Études Spatiales, 2 Place Maurice Quentin, 75039 Paris cedex 1, France*

Accepted 10 August 2002

Abstract

Launched on 23rd February 1999, the Ørsted satellite opened the decade of geopotential field research. This is the first satellite to measure the three components of the Earth's magnetic field since MAGSAT (1979–1980). Ørsted orbital parameters are very similar to those of MAGSAT, allowing a first-order comparison of the 1979 and 2000 magnetic fields. Using the available vector and scalar data over the first 14 months of the Ørsted mission and applying classical selection criteria (local time, external magnetic activity), we compute a 29-degree/order main-field model and a 13-degree/order secular-variation model for the period 1999–2000. The applied method and the accuracy of the derived model are discussed. We compare the resulting main-field model to a similar one derived from MAGSAT data. Results of this comparison are presented, such as (i) morphology and energy spectrum of the secular variation and (ii) morphology of the crustal magnetic field at MAGSAT and Ørsted epochs.
© 2003 Elsevier Science B.V. All rights reserved.

Keywords: Magnetic field; Satellite data; Modeling

1. Introduction

In the quest to understand the structure and dynamical processes in the Earth's deep interior, one of the most important sources of information is knowledge of the Earth's magnetic field and its evolution in time. Changes in the main magnetic field with time, known as secular variation, have been recognized since Henry Gellibrand compared magnetic declination measurements he made in London in 1634 with measurements made by Gunter and Borough 12 and 54 years before (Malin and Bullard, 1987). From the mid-19th century onwards, detailed and accurate information about secular variation became available from the magnetic observatories which continuously measured the geomagnetic field (Langel, 1987). Unfortunately, the global observatory network provides magnetic data only at a finite number of unevenly distributed locations. Accuracy of the global main-field and secular-variation models relies, among other parameters, on the geographic data distribution (Alexandrescu et al., 1994; Langel et al., 1995; Langlais and Mandea, 2000) and is thus limited.

The advent of the space age provided the opportunity to obtain such an ideal dataset by launching satellites that carry vector magnetometers. The first satellite mission dedicated to this task was MAGSAT, which operated from November 1979 to May 1980. Unfortunately, while this mission provided the most accurate model of the geomagnetic field at that particular

* Corresponding author. Tel.: +1-301-614-6455; fax: +1-301-614-6522.
E-mail address: langlais@geomag.gsfc.nasa.gov (B. Langlais).

0031-9201/03/$ – see front matter © 2003 Elsevier Science B.V. All rights reserved.
doi:10.1016/S0031-9201(02)00207-8

time period, it did not last long enough to provide an accurate model of the secular variation (Barraclough, 1985). Following MAGSAT, the geomagnetic community waited for 20 years before the successful launch and deployment of the Ørsted satellite, that provides data of a similar quality to MAGSAT, allowing a second highly accurate snapshot of the geomagnetic field. This latest satellite not only allows us to refine our knowledge of the main field, but also provides the opportunity to study its evolution over 20 years. Furthermore, the 14 months of Ørsted data used here are long enough to construct secular-variation models.

MAGSAT and Ørsted having nearly the same orbital parameters (except for the altitude), it is straightforward to make first-order comparisons between main-field models computed from both satellites data. In the following, we first summarize the modeling methodology, together with the applied weighting schemes. The method is then applied to the selected MAGSAT and Ørsted datasets. Resulting main-field models (for 1979 and 2000) and the mean (1979–2000) and instantaneous (1999–2000) secular-variation models are presented. We then discuss the accuracy of the different models. We finally compare the magnetic field models between MAGSAT and Ørsted epochs, with regard to both the temporal evolution of the main field and the lithospheric field.

2. Determining a field model

2.1. Mathematical expression

The magnetic field $\vec{B}$ can be expressed as $\vec{B} = -\vec{\nabla} V$, where V is a scalar potential satisfying $\Delta V = 0$. This potential is the sum:

$$V = V_{\text{int}} + V_{\text{ext}} \tag{1}$$

where V_{int} and V_{ext} are the internal and external scalar potentials, respectively. These two potentials can be represented by spherical harmonic expansions, following Gauss (1839):

$$V_{\text{int}} = a \sum_{n=1}^{N_{\text{i}}^{\max}} \left(\frac{a}{r}\right)^{n+1} \sum_{m=0}^{n} (g_n^m \cos(m\phi) + h_n^m \sin(m\phi)) P_n^m(\cos(\theta)) \tag{2}$$

$$V_{\text{ext}} = a \sum_{n=1}^{N_{\text{e}}^{\max}} \left(\frac{r}{a}\right)^{n} \sum_{m=0}^{n} \left(q_n^m \cos(m\phi) + s_n^m \sin(m\phi)\right) P_n^m(\cos(\theta)) + Dst \sum_{n=1}^{1} \left[\left(\frac{r}{a}\right)^{n} + Q_1 \left(\frac{a}{r}\right)^{n+1}\right] \times \sum_{m=0}^{n} (\tilde{q}_n^m \cos(m\phi) + \tilde{s}_n^m \sin(m\phi)) P_n^m(\cos(\theta)) \tag{3}$$

where the reference radius is $a = 6371.2$ km, corresponding to the mean radius of the Earth, and r, θ, ϕ are the radial distance, the geocentric colatitude and the longitude of a given measurement location, respectively. $P_n^m(\cos\theta)$ and are the Schmidt-normalized associated Legendre functions of degree n and order m. Measurements of the magnetic field are used to estimate the so-called Gauss spherical harmonic coefficients ((g_n^m, h_n^m) for internal sources, and (q_n^m, s_n^m) for external sources), which in principle uniquely describe the geomagnetic field outside the sources region. Eqs. (2) and (3) are truncated to $N_{\text{i}}^{\max}$ and $N_{\text{e}}^{\max}$, respectively. The coefficients ($\sim q_1^0$, $\sim q_1^1$, $\sim s_1^1$) account for the first-degree and order *Dst*-dependent part of the external field, with its internal induced counterpart represented by Q_1.

The Gauss coefficients are also time-dependent. Indeed, the temporal variations of the geomagnetic field have an extremely wide spectrum, ranging over more than 20 orders of magnitude (Courtillot and Le Mouël, 1988). In order to recognize time variations of internal origin, the secular variation, one needs about 1 year of continuous observations. This variation is assumed to be constant over short time scales. Secular variation can be introduced in Eq. (2) by adding a secular-variation potential, V_{sv}, truncated to $N_{\text{sv}}^{\max}$:

$$V_{\text{sv}} = a \sum_{n=1}^{N_{\text{sv}}^{\max}} \left(\frac{a}{r}\right)^{n+1} \sum_{m=0}^{n} (t - T_0)(\dot{g}_n^m \cos(m\phi) + \dot{h}_n^m \sin(m\phi)) P_n^m(\cos(\theta)) \tag{4}$$

where $\dot{g}_n^m$ and $\dot{h}_n^m$ are the time derivatives of the internal Gauss coefficients. T_0 denotes the reference time (i.e. the epoch of the main-field model), and t is the considered time.

First, we consider different maximum degrees for the secular-variation and main-field models. Usually the secular variation is solved only for the first 8 degrees, and neglected above, as for the IGRF models (Mandea and Macmillan, 2000). Solving for the high-degree, low-energy terms is not easy because some overlapping appears in both spatial and temporal domains, between crustal field and secular variation. A second approach is thus considered. The low-degree secular-variation coefficients are solved together with the main-field coefficients, and the high-degree terms are set to a priori estimated values. This removes the corresponding part of secular variation V_{svp} from the observations, using:

$$V_{\mathrm{svp}} = a \sum_{n=N_{\mathrm{sv}}^{\min}}^{N_{\mathrm{sv}}^{\max}} \left(\frac{a}{r}\right)^{n+1} \sum_{m=0}^{n} (t - T_0) \left(\dot{g}_n^m \cos(m\phi) + \dot{h}_n^m \sin(m\phi)\right) P_n^m(\cos(\theta)) \quad (5)$$

Secular-variation coefficients for $n < N_{\mathrm{sv}}^{\min}$ are solved, the ones for $N_{\mathrm{sv}}^{\min} \leq n \leq N_{\mathrm{sv}}^{\max}$ are set to a priori coefficients, and the last ones (if $N_{\mathrm{sv}}^{\max} < N_{\mathrm{i}}^{\max}$) are assigned zero.

In the present study, geomagnetic external variations, such as the daily variation, the apparent 27-day periodicity in magnetic activity, the semi-annual and annual variations, and the approximate 11-year period variations, are neglected.

2.2. General solution

The observed components (C_i^{obs}) of the ith magnetic field measurements $\vec{B}_i^{\mathrm{obs}}$ are the northward (X_i^{obs}), eastward (Y_i^{obs}), downward vertical (Z_i^{obs}) components, and total intensity (F_i^{obs}). They are used to estimate the spherical harmonic coefficients, by minimizing the sum (Cain et al., 1967):

$$\chi^2 = \sum_{i=1}^{\mathbb{N}_{\mathrm{obs}}} \omega_i^C \left(C_i^{\mathrm{obs}} - C_i^{\mathrm{mod}}\right)^2 \quad (6)$$

where C_i^{mod} is the corresponding field component derived from the model, $\mathbb{N}_{\mathrm{obs}}$ is the number of observations and ω_i^C denotes the weight associated to the ith measured component.

When considering an isotropic source of error, ω_i^C is commonly set to $1/\sigma_i^2$, where σ_i is the estimated measurement accuracy. This weighting scheme can be also expressed as a function of local time (to downweight dayside data), or of the geographical position (to downweight polar data). Identical weights are used whatever field component X, Y or Z is considered. This is the approach we applied to MAGSAT data, but not to Ørsted data.

For Ørsted, the poor determination of the rotation angle around the pointing axis ($\hat{n}$) of the Star IMager (SIM) leads to anisotropic uncertainties (Olsen et al., 2000). Resulting errors on the field components are thus anisotropic, which are taken into account by a weighting scheme developed by Holme and Bloxham (1996). $\vec{B}$, the observed magnetic field vector, and $\hat{n}$ can be used to define a new reference frame in which errors on each field components can be expressed (provided their directions are not parallel). The new coordinate system is defined by $\vec{B}$, $\hat{n} \wedge \vec{B}$ and $\vec{B} \wedge (\hat{n} \wedge \vec{B})$, to which we refer as B, $B_\perp$ and B_3, respectively (Holme, 2000). The solution is obtained by solving Eq. (6), using the field components expressed in the new reference frame. Individual weights in this new coordinate system are:

$$\omega^B = \frac{1}{\sigma^2} \quad (7)$$

$$\omega^{B_\perp} = \frac{1}{\sigma^2 + (\hat{n} \wedge \vec{B})^2 \xi^2 + (\hat{n} \times \vec{B})^2 \psi^2} \quad (8)$$

$$\omega^{B_3} = \frac{1}{\sigma^2 + B^2 \psi^2} \quad (9)$$

where ψ^2 and ξ^2 are error variances parallel and perpendicular to $\hat{n}$.

For a near-polar orbiting satellite, the number of data is larger near the poles than near the equator. Such an uneven coverage can be counterbalanced either by selectively decimating data along orbits or by downweighting data using a $\sin(\theta)$ factor (the latest one was chosen in this study). Weights are finally normalized to get their sum for scalar (or vector) data equal to the total number of scalar (or vector) data.

3. Modeling

Below we present the selection criteria applied to both MAGSAT and Ørsted magnetic measurements. Using MAGSAT subsets, we looked for the optimal

interval during which the main field can be recovered, while the secular variation can be neglected. Afterwards, we used identical time periods for Ørsted subsets, and then computed a model based on the whole Ørsted dataset.

3.1. Data selection

MAGSAT flew 7 months during 1979 and 1980. The available dataset contains three-component measurements, sampled at 2 Hz. For Ørsted, scalar and vector data of level 2.2 available from March 1999 to April 2000 were used. From May to November 2000, the full solar illumination led to malfunction of the SIM so that no vector data are available (Kim Bisgaard, ØSDC, personal communication). We considered both vector magnetometer (CSC) and scalar magnetometer (OVH) data. At the time of writing, these data remain provisional, having rare but large time jumps. Outliers were removed by comparing measurements with values predicted by the derived model (Langlais et al., 1999).

To limit the influence of external field variations, only the dawn side data were selected from the MAGSAT mission and only night time data from the Ørsted mission (corresponding to the North-to-South passes, with local time over the equator slowly decreasing from 3:00 to 20:00). Filtering was then applied to both satellites datasets by using external activity indices: considering a particular data with associated time t (in hour), the criteria used are $Kp(t) \leq 1^+$, $Kp(t \pm 3) \leq 2^-$, $|Dst| \leq 5\,\mathrm{nT}$, $|\mathrm{d}(Dst)/\mathrm{d}t| \leq 3\ \mathrm{nT\,h^{-1}}$. These criteria are more restrictive than those used for the Ørsted Initial Field Model (OIFM) by Olsen et al. (2000), but the resulting dataset is large enough to allow the high-degree and order spherical harmonic models to be derived. At high absolute dipole latitude (>50°), only intensity data were used; in the following priority was given to OVH measurements; when missing, computed values from the CSC measurements were used.

All the derived models were computed with different values for $N_\mathrm{i}^\mathrm{max}$, with $N_\mathrm{e}^\mathrm{max} = 2$, and with a first-degree Dst-dependence (with $Q_1 = 0.27$ (Langel and Estes, 1985)). We used an isotropic weighting scheme for MAGSAT ($\sigma = 4\,\mathrm{nT}$), and an anisotropic one for Ørsted ($\sigma = 4\,\mathrm{nT}$, $\psi = 10''$ and $\xi = 60''$).

3.2. Modeling the MAGSAT data

In this study the geomagnetic field is modeled using only satellite data. Because the MAGSAT satellite provided only 6 months of magnetic measurements, the secular variation over this short time interval can be recovered only if the external, periodic variations are minimized (Cain et al., 1983). However, modeling the secular variation from MAGSAT data is controversial (Barraclough, 1985). In the following we analyze in more detail the secular-variation modeling over short time periods.

A crucial point is the choice of the shortest time interval during which the main field can be well determined while the secular-variation effects can be neglected. We used the MAGSAT dataset to define this optimal time interval. Noting g the internal field coefficients, we made the distinction between $\partial g/\partial t$ (computed together with g) and $\Delta g/\Delta T = (g_2 - g_1)/(T_2 - T_1)$ (computed as the difference between two consecutive g).

We first tested the data distribution as a function of time duration by increasing the time intervals. Data were sorted onto a $3^\circ \times 3^\circ$ equiangular grid to homogenize the consecutive datasets. As the derived models are truncated to $N_\mathrm{i}^\mathrm{max} = 20$, an equiangular distribution with one point per $12^\circ \times 12^\circ$ bin is required. For 1, 1.5, 2 and 3 months, bins were filled to 90.1, 95.5, 99.9 and 100%, respectively, suggesting that models derived with less than a 1.5-month time interval might not be reliable.

Table 1 presents the first-degree and order secular-variation coefficients based on different time interval datasets. Comparing $\partial g/\partial t$ and $\Delta g/\Delta T$, it is possible to evaluate the optimal time interval during which (i) $\partial g/\partial t$ are uncorrelated between successive models, and (ii) $\Delta g/\Delta t$ are close to the expected values given by an a priori model. Models based on 1-month and 1.5-month datasets are unrealistic: both $\partial g/\partial t$ and $\Delta g/\Delta T$ are uncorrelated and reach several tens of nT. The 2-month models provide uncorrelated $\partial g/\partial t$ coefficients, while $\Delta g/\Delta T$ are more realistic when compared to the DGRF 1980 coefficients (Barraclough, 1987) or to the ones of the M102389 model (Cain et al., 1989). The secular variation $\partial g/\partial t$ is significant over the 3-month time interval, and thus should not be ignored.

Table 1
First-degree and order secular-variation coefficients (in nT per year) derived together with g (left columns) and computed as the difference between consecutive g (right columns)

$\partial g_1^0/\partial t$	$\partial g_1^1/\partial t$	$\partial h_1^1/\partial t$	Time period	$\Delta g_1^0/\Delta T$	$\Delta g_1^1/\Delta T$	$\Delta h_1^1/\Delta T$
75.3	5.8	−43.0	01/11/1979 → 30/11/1979	67.1	85.8	−94.5
57.0	55.1	−18.4	01/12/1979 → 31/12/1979	−13.8	−37.7	31.3
−19.2	35.4	24.4	01/01/1980 → 31/01/1980	14.1	−17.1	−22.6
−8.3	12.8	59.8	01/02/1980 → 29/02/1980	−34.1	18.1	14.1
26.7	−57.8	21.8	01/03/1980 → 31/03/1980	85.6	−49.7	−63.1
57.8	−2.0	−98.9	01/04/1980 → 30/04/1980			
47.4	21.7	−57.1	01/11/1979 → 15/12/1979	25.3	27.9	−24.8
1.2	3.4	4.3	16/12/1979 → 31/01/1980	14.4	−3.6	−2.3
22.7	4.1	−8.7	01/02/1980 → 15/03/1980	54.5	−4.2	−30.6
41.6	9.2	−68.0	15/03/1980 → 30/04/1980			
43.7	40.0	−57.8	01/11/1979 → 31/12/1979	19.1	7.1	−19.0
11.9	−3.5	−13.1	01/01/1980 → 29/02/1980	29.7	13.9	−10.8
35.6	5.6	−39.9	01/03/1980 → 30/04/1980			
24.4	17.1	−28.5	01/11/1979 → 31/01/1980	20.1	9.3	−11.4
26.6	11.0	−20.8	01/02/1980 → 30/04/1980			
23.8	11.3	−19.0	01/11/1979 → 30/04/1980			
25.0	14.9	−17.4	Cain et al. (1989)			
23.6	10.2	−20.8	Barraclough (1987)			

However, it should be tested whether secular variation can be ignored over 2-month interval. We thus compared the rms (derived from χ^2 in Eq. (6)) for models computed with and without secular variation. The improvement of the rms is only 1.7, 1.2, 4.4 and 4.5% for X, Y, Z and F, respectively. The residuals in F are twice as large as those of the X, Y and Z components, but the intensity measurements were used mostly near the polar area, where the external magnetic field presents short time period variations.

Finally, the 2-month models without solving for the secular variation were retained to represent the magnetic field. These models are named with respect to the time period considered, namely M19791112 for November and December 1979, M19800102 for January and February 1980, and M19800304 for March

Table 2
Number of scalar $\mathbb{N}_{sca}$ and of vector $\mathbb{N}_{vec}$ data and rms misfits (σ in nT) of the derived models

Model	$\mathbb{N}_{sca}$	$\sigma(F)$	$\mathbb{N}_{vec}$	$\sigma(B)$	$\sigma(B_\perp)$	$\sigma(B_3)$	$\sigma(B_r)$	$\sigma(B_\theta)$	$\sigma(B_\phi)$
M19791112	37690	8.9	43688				4.9	6.7	6.6
M19800102	38226	8.1	36316				5.3	7.3	6.5
M19800304	29922	8.1	34469				5.3	6.5	5.7
Ø19990304	71118	3.9	6372	2.4	7.6	2.7	4.1	5.1	5.2
Ø19990506	65566	6.3	10655	3.2	8.7	3.3	5.2	6.4	5.3
Ø19990708	42940	5.8	8577	2.4	8.6	3.3	5.3	6.5	4.6
Ø19990910	24144	6.1	11208	2.4	8.4	3.3	5.2	6.1	4.9
Ø19991112	38868	6.5	21791	2.1	7.6	3.0	4.6	5.2	5.0
Ø20000102	35454	6.2	18990	2.7	8.3	3.0	4.9	5.8	5.3
Ø20000304	46538	4.5	20613	2.4	7.6	4.9	4.9	5.0	5.6
Ø19992000_SVM	323953	6.7	97530	3.6	8.6	4.3	5.2	6.9	5.6
Ø19992000_SVI	323953	6.6	97530	3.6	8.6	4.3	5.2	6.9	5.6

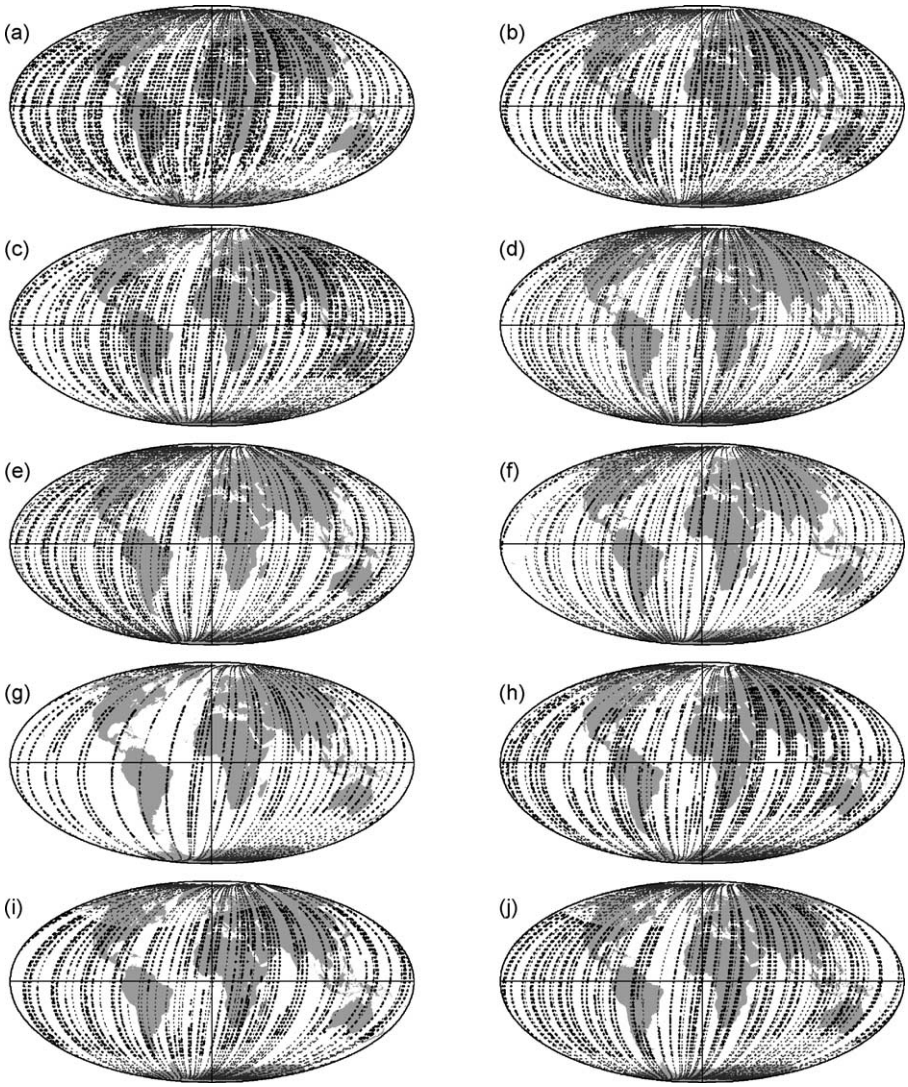

Fig. 1. Geographical distribution of scalar (gray) and vector (black) satellite data. From (a) to (j), M19791112, M19800102, M19800304, Ø19990304, Ø19990506, Ø19990708, Ø19990910, Ø19991112, Ø20000102 and Ø20000304.

and April 1980. The rms of these models are shown in Table 2 and the geographical distribution of the data is shown in Fig. 1. The mean of these three models is named M19791980_SV0.

3.3. Modeling the Ørsted data

Comparison of MAGSAT and Ørsted models is possible if the same criteria are applied in both data selection and model parameterization. We decimated the Ørsted 14-month dataset into seven 2-month subsets. Each of these 2-month subsets was tested with respect to the data geographical distribution (Fig. 1). Considering a $12^\circ \times 12^\circ$ equiangular grid, 98.4% of the bins were filled. We then computed seven models: Ø19990304, Ø19990506, Ø19990708, Ø19990910, Ø19991112, Ø20000102 and Ø20000304, whose rms values are listed in Table 2. The mean of these seven 2-month models is denoted Ø19992000_SV0 (with resulting parameters $N_{\mathrm{i}}^{\max} = 20$ and $N_{\mathrm{sv}}^{\max} = 0$).

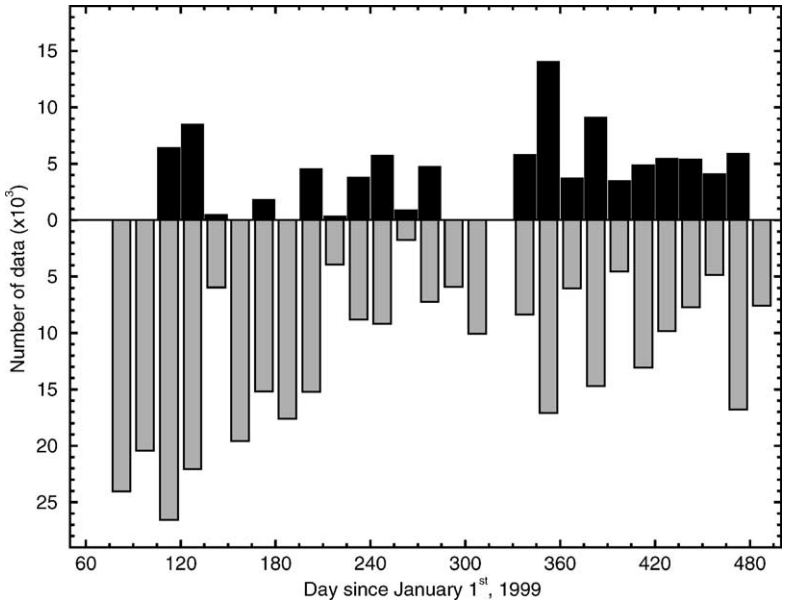

Fig. 2. Time distribution of Ørsted data. Data are counted during 15-day periods. Upper and lower panels show scalar and vector time distributions, respectively.

We combined the seven subsets to have a complete 14-month dataset. Fig. 2 shows the data distribution with respect to time. In this new case the data distribution of the 14-month filled a $6^\circ \times 6^\circ$ equiangular grid. Moreover, this dataset contained almost one measurement per $12^\circ \times 12^\circ$ bin for every 2-month interval (due to the previously described data selection). We computed two models based on the 14-month dataset—both are truncated to $N_i^{max} = 29$, with the same external parameters as above. The first model was computed with $N_{sv}^{min} = N_{sv}^{max} = 13$, i.e. with instantaneous secular variation. This model is denoted Ø19992000_SVI. The second model, denoted Ø19992000_SVM, was computed with $N_{sv}^{min} = 8$ and $N_{sv}^{max} = 13$, i.e. with mixed secular variation. The input secular-variation model is the average of the differences between the MAGSAT and Ørsted models. The associated rms of Ø19992000_SVI and Ø19992000_SVM models are given in Table 2.

4. Quality of the models

We compared Ø19992000_SVI and Ø19992000_SVM to previously published magnetic field models for the same epoch. We considered the International Geomagnetic Reference Field 2000 (IGRF 2000) and Ørsted Initial Field Model (OIFM). IGRF 2000 (Mandea and Macmillan, 2000) is truncated to $N_i^{max} = 10$ and $N_{sv}^{max} = 8$, with no external terms. This model is predictive and is based on different datasets, including ground and satellite observations. OIFM (Olsen et al., 2000) is truncated to $N_i^{max} = 19$, $N_e^{max} = 2$, with no secular variation. This model is built using Ørsted data spanning a short time interval.

The models were tested whether they could properly predict the Ørsted 14-month magnetic measurements. To make the tests independent with respect to the external field parameterization, the external coefficients and the first-degree and order *Dst*-dependence were assumed to be constant and equal to those of Ø19992000_SVI.

Results are expressed in terms of rms between observed and predicted magnetic field values (Table 3). The most interesting result is that both the Ø19992000_SVI and Ø19992000_SVM models better predict the field observations than the OIFM. Comparisons with the IGRF 2000 main-field model (not shown) lead to similar conclusions. The rms of tests 1, 2 and 3 (Table 3) demonstrate that our

Table 3
Residuals (in nT) computed for different models and truncations

Test	Input MF	N_i^{max}	Input SV	N_{sv}^{max}	$\sigma(F)$	$\sigma(B)$	$\sigma(B_\perp)$	$\sigma(B_3)$
1	OIFM	14	IGRF 2000	8	9.97	5.04	8.69	5.00
2	Ø19992000_SVI	14	IGRF 2000	8	8.81	4.79	8.71	4.76
3	Ø19992000_SVM	14	IGRF 2000	8	8.77	4.78	8.72	4.75
4	OIFM	14	Ø19992000_SVI	8	8.43	4.44	8.70	4.86
5	Ø19992000_SVI	14	Ø19992000_SVI	8	6.97	3.69	8.58	4.50
6	OIFM	14	Ø19992000_SVI	13	8.25	4.44	8.70	4.84
7	Ø19992000_SVI	14	Ø19992000_SVI	13	6.78	3.68	8.59	4.48
8	OIFM	14	Ø19992000_SVM	8	8.51	4.45	8.69	4.86
9	Ø19992000_SVM	14	Ø19992000_SVM	8	6.91	3.70	8.60	4.49
10	OIFM	14	Ø19992000_SVM	13	8.51	4.45	8.69	4.86
11	Ø19992000_SVM	14	Ø19992000_SVM	13	6.91	3.69	8.60	4.49
12	Ø19992000_SVI	26	Ø19992000_SVI	13	6.58	3.59	8.57	4.37
13	Ø19992000_SVM	26	Ø19992000_SVM	13	6.72	3.60	8.58	4.38

main-field models, truncated to $N_i^{max} = 14$, are better than the OIFM, while there are little differences between Ø19992000_SVI and Ø19992000_SVM. Runs numbered 4, 5, 8 and 9 test secular variation truncated to $N_{sv}^{max} = 8$, while runs 6, 7, 10 and 11 test the full secular-variation models. On one hand, our secular-variation models appear to be more accurate than the IGRF 2000, while on the other hand, the higher degree of truncation has only little influence on the residuals. Statistics on Ø19992000_SVI and Ø19992000_SVM truncated to $N_i^{max} = 26$ from tests 12 and 13 give similar results, except for the total intensity where the differences are ≈2%.

All these results confirm that Ø199920000_SVI and Ø19992000_SVM are more reliable than previously published models. However, these tests do not allow discrimination between the instantaneous and mixed secular-variation models, which we then looked for.

To get more information on the accuracy of the models we computed the energy spectra (Lowes, 1974) for all models described above. Fig. 3 shows these spectra for (a) MAGSAT and (b) Ørsted models. The energy spectra show similar behavior up to degree 14 for the MAGSAT 2-month models. The Ørsted 2-month models are similar up to degree 10. After these limits, the spectra are more dispersed, spanning nearly one or two orders of magnitude for MAGSAT or Ørsted models, respectively. This discrepancy in the Ørsted models is due to poorer geographic data distribution, especially for Ø19990708 and Ø19990910, datasets with gaps exceeding some tens of degrees above the equator (Fig. 1).

Much more information can be extracted from Fig. 4a, where 14-month internal field models spectra are shown. These spectra are similar up to degree 14. Thereafter, only Ø19992000_SVI and Ø19992000_SVM exhibit the same behavior. Fig. 4a also shows the spectrum of the Ø19992000_SV0 rms, obtained as the differences between this model and the 2-month Ørsted models. Those rms are used to estimate the rms for Ø19992000_SVI and Ø19992000_SVM models. Field and rms spectra intersect near degree 15, which indicates that our internal field models are reliable at least up to this degree.

It is worth noting that Ø19992000_SVI internal field model is slightly more energetic at $N_i = 13$ than Ø19992000_SVM. This difference is likely linked to the way secular variation is parameterized. Fig. 4b shows spectra of the mean, instantaneous and mixed secular-variation models. It also introduces the energy spectrum of the 1989 secular-variation model calculated from Bloxham and Jackson (1992), denoted as BJ1989. The differences between Ø19992000_SVI and Ø19992000_SVM are important, reaching three orders of magnitude at degree 13; the same difference is observed between Ø19992000_SVM and BJ1989. The Ø19992000_SVI secular-variation energy between degrees 8 and 13 is at the same energy level as the Ø19992000_SV(I–M) internal field ones (Fig. 4a).

All these tests underline the similarity of the Ø19992000_SVI and Ø19992000_SVM internal field models. However, the secular-variation coefficients

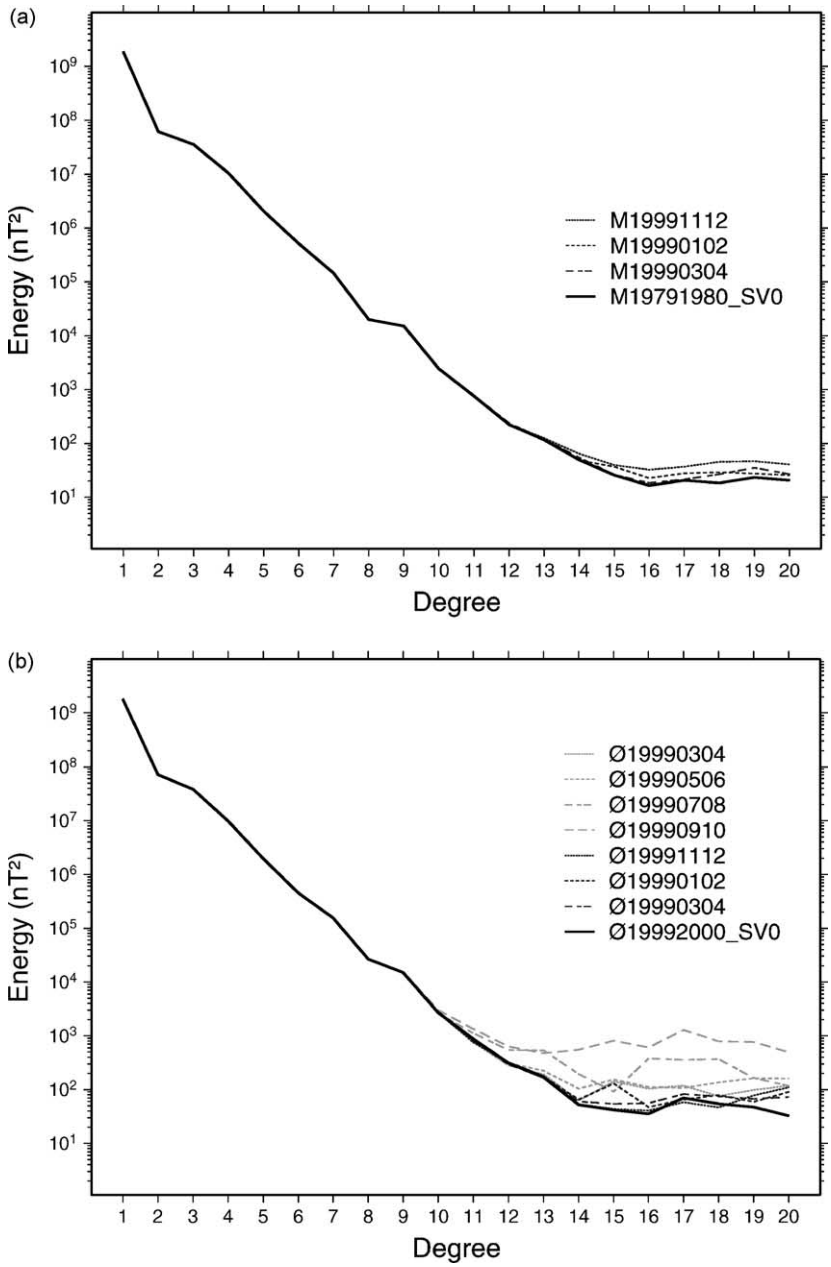

Fig. 3. Energy spectra of (a) the three MAGSAT main-field models and of (b) seven Ørsted main-field models. Spectra of the M19791980_SV0 and Ø19992000_SVO mean models are also shown.

show large differences, which do not reflect the improvement of the modeling with respect to the computed rms presented in Table 2. We therefore consider the Ø19992000_SVM model as the most accurate one.

5. Discussion

In this section, the geomagnetic field models described above are used to discuss the secular-variation

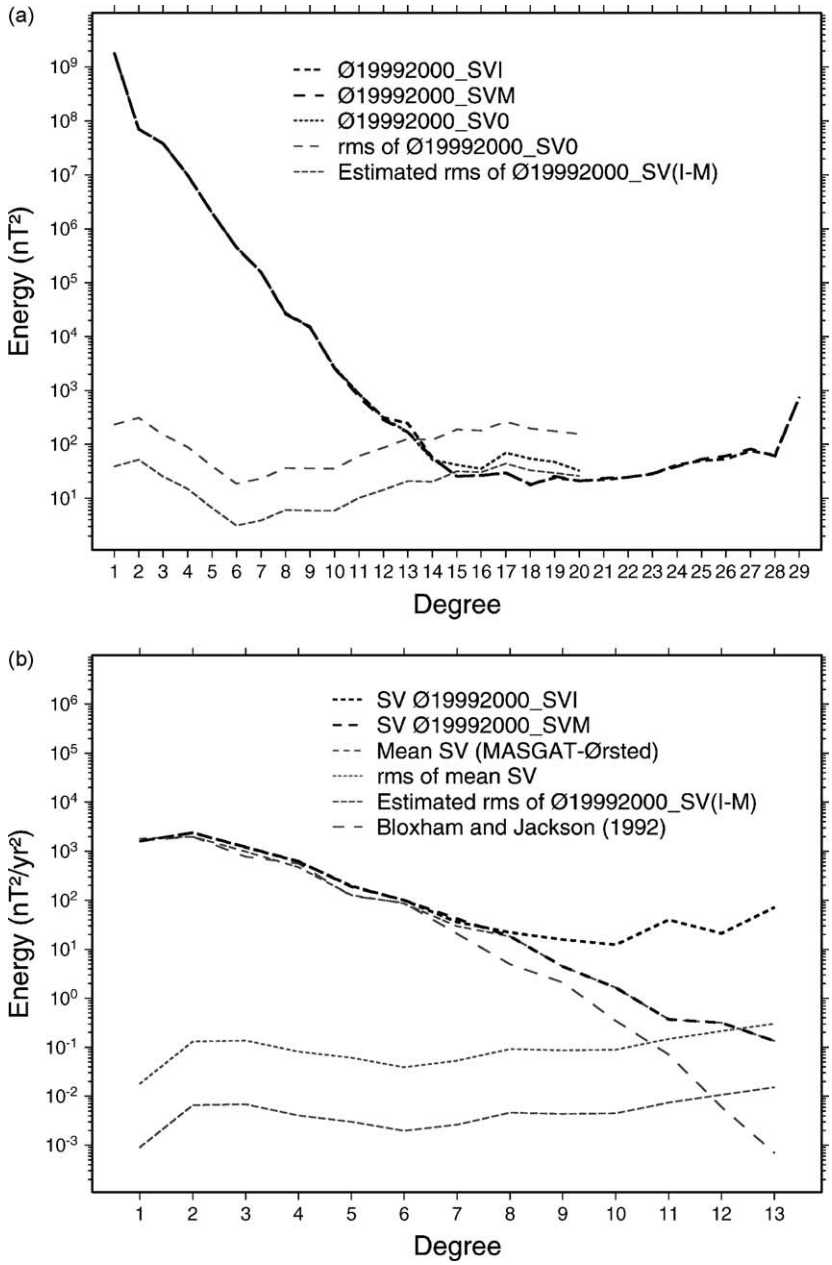

Fig. 4. Energy spectra of (a) main-field models and associated rms, and (b) secular-variation models and associated rms.

behavior at the Earth's surface and at the core–mantle boundary, as well as the geomagnetic lithospheric field as predicted by Gauss coefficients (above degree and order 13).

5.1. Temporal variations

Previous secular-variation models were essentially based on ground measurements. The uneven temporal

and spatial distribution of ground data usually led to the truncation of secular-variation models to low degrees and orders. Thus, knowing the secular variation up to degree and order 13 is important to better understand the short-term variations of the main magnetic field. The advent of the Ørsted satellite has brought major improvements: the energy spectrum of our model clearly confirms the core origin of the secular variation up to degree and order 13. The temporal variation for higher degree is not well determined, as it is overlapped by the crustal magnetic field.

Fig. 5 shows the secular variation intensity at the Earth's surface, predicted by (a) IGRF 2000 (Mandea and Macmillan, 2000) and (b) Ø19992000_SVM up to degree and order 8. The large-scale behavior of the secular variation is the same for both, although the observed amplitudes of the secular variation from the Ø19992000_SVM are larger than those predicted by IGRF 2000. The Ørsted satellite considerably improves our knowledge of the secular variation. Fig. 5d shows the differences between IGRF 2000 and Ø19992000_SVM to $N_i = 8$. These differences reach some tens of nT in some areas (above the western Pacific ocean); the rms differences are equal to 18.66 nT per year. The secular variation predicted by Ø19992000_SVM to $N_i = 13$ looks very similar (Fig. 5c), with rms differences between degrees 8 and 13 equal to 1.56 nT per year, only. However, previous high-degree and order secular-variation models, as Bloxham and Jackson (1992) are not characterized by the same energy level as Ø19992000_SVM (Fig. 4b). The observed rapid decrease in secular-variation power about degree 8 is due to the lack of information in the data to constrain the model above this degree; the solution is controlled by the regularizing norm.

We have shown that the MAGSAT and Ørsted satellite missions provide a good database to produce better secular-variation models, which can be used to study the Earth's deep interior. One possible application is to estimate the radius of the Earth's liquid core from geomagnetic model and to compare it with the seismologically constrained value (3486 ± 5 km).

The method applied here was detailed by Hide (1978) and is now summarized. Secular variation $\partial\vec{B}/\partial t$ inside a conducting fluid is driven by the fluid

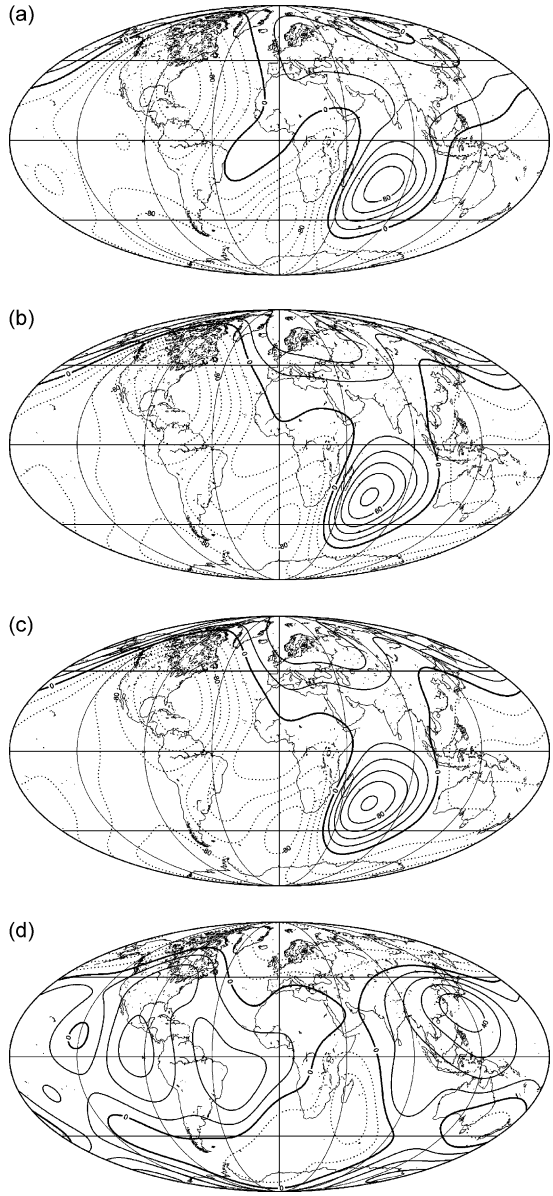

Fig. 5. Amplitude of the secular variation at the Earth's surface: (a) IGRF 2000 up to $N_i = 8$; (b) Ø19992000_SVM up to $N_i = 8$; (c) Ø19992000_SVM up to $N_i = 13$ (Contours 20 nT per year); (d) difference between IGRF 2000 and Ø19992000_SVM up to $N_i = 8$ (Contours 10 nT per year).

velocity $\vec{u}$:

$$\frac{\partial \vec{B}}{\partial t} = \vec{\nabla} \wedge (\vec{u} \wedge \vec{B}) + (\mu\sigma)^{-1} \Delta \vec{B} \tag{10}$$

The two members of the magnetic induction equation correspond to advection and diffusion. Diffusion is controlled by the permeability (μ) and the conductivity (σ) of the core. The diffusion is neglected over historical time scales, which leads to the frozen flux assumption. At the core–mantle boundary, the radial component of Eq. (10) is:

$$\frac{\partial B_r}{\partial t} = -\vec{\nabla}_{\mathrm{H}} \times (\vec{u} B_r) \tag{11}$$

where $\vec{\nabla}_{\mathrm{H}} = \vec{\nabla} - \vec{n}(\partial/\partial r)$, $\vec{n}$ denotes the unit radial outward vector.

Assuming a closed surface S_i at the core–mantle boundary delimited by $B_r = 0$, then Eq. (11) is equivalent to (Backus, 1968):

$$\delta F = \int_{S_i} \frac{\partial B_r}{\partial t} \mathrm{d}S = 0 \tag{12}$$

or

$$\Delta F = \frac{\mathrm{d}}{\mathrm{d}t} \int_{S_i} B_r \, \mathrm{d}S = 0 \tag{13}$$

Eqs. (12) and (13) can be used for the whole core–mantle boundary surface, and we can thus estimate the magnetic core radius (R_N) as a function of the degree N_{i} of truncation. We present three cases, the first one based on $\Delta F = 0$, and the two others based on $\delta F = 0$. We successively used (i) M19791980_SV0 and Ø19992000_SVM, (ii) Ø19992000_SVI and (iii) Ø19992000_SVM. Estimated core radii for different truncation degrees are presented in Table 4.

Table 4
Estimated liquid core radius (in km) for different degrees of truncation

Models	R_{11}	R_{12}	R_{13}	R_{14}
M19791980_SV0 Ø19992000_SVM	3580.5	3714.2	3690.7	3656.0
Ø19992000_SVI	3760.0	3786.0	4098.0	4327.0
Ø19992000_SVM	3555.1	3681.8	3661.2	3587.6

Radii computed from Ø19992000_SVI correspond to minimum values for Eq. (12). The seismologically constrained radius is 3486 ± 5 km.

The estimated values are systematically greater than the seismic value. There are no solutions for Ø19992000_SVI whatever the N_{i}: the values in Table 4 were calculated when ∂F was at minimum. Radii computed from M19791980_SV0 and Ø19992000_SVM, and from Ø19992000_SVM are similar, with R_{12} and R_{13} larger than R_{11} and R_{14}, these latter radii being closer to the seismic value. However, R_{11} is computed by neglecting some core Gauss coefficients. On the contrary, R_{14} is probably biased by lithospheric terms. Overestimates may be related to some core and crustal overlapping between degrees 11 and 14. Our Ø19992000_SVM secular-variation model may have too much energy at degrees 12 and 13.

5.2. Crustal field

The Ø19992000_SVM model also helps to better characterize the crustal magnetic field. Fig. 6 shows the amplitudes of the crustal field contributions derived from our model and from the M102389 MAGSAT model (Cain et al., 1989), drawn at Ørsted mean altitude (740 km). In each case, the crustal field is computed as the difference between predicted data up to $N_{\mathrm{int}} = 26$ and predicted data up to $N_{\mathrm{int}} = 13$. The difference between predicted crustal field from MAGSAT and from Ørsted models is also shown.

Some well-known magnetic anomalies are well defined on both maps: the Bangui and Kursk anomalies, the North America craton, the South West of Australia, South Africa, North of New Zealand, and the Himalayan chain. Magnetic anomalies are in general weaker over oceanic areas (especially above the eastern Pacific ocean). Generally speaking, the anomalies trend dominantly North–South in the Ørsted model compared to MAGSAT one. The largest discrepancies are mostly located in the Southern Hemisphere. This behavior could be partly explained by the known deficiency of the SIM to properly restore the satellite attitude over the South Atlantic Anomaly (Olsen et al., 2000). The mean altitudes of the Ørsted measurements (Fig. 6d) indicate a correlation between these discrepancies and the highest altitudes (especially above the Indian Ocean). Furthermore, the alternation of high and low passes, especially over the South Pacific Ocean, could explain the North–South lineation of the observed crustal contributions. The large differences occurring near the poles are linked to

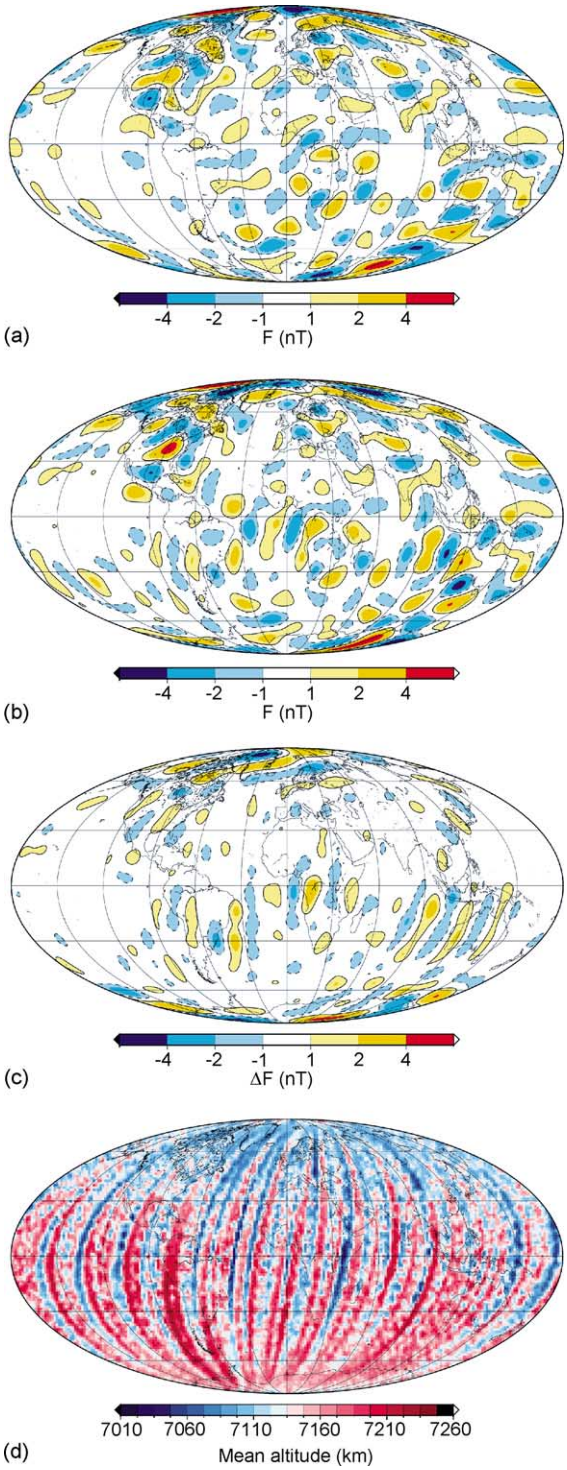

the inclination of the satellites (96.76° for MAGSAT and 96.62° for Ørsted), thus no polar data are available.

We estimated the correlation coefficients between maps (Fig. 6a and b). The correlation between MAGSAT and Ørsted crustal contributions at 740 km is 0.71, but increases to 0.74 for latitudes between ±75°, and to 0.78 for latitudes between ±60°. Within this latitude band, the rms difference between MAGSAT and Ørsted charts is 0.75 nT. The crustal field predicted by Ø19992000_SVM (between $N_{\text{int}} = 14$ and 26) is highly correlated with the crustal field observed by MAGSAT in 1979–1980, although MAGSAT flew closer to the sources, and the actual accuracy of Ørsted measurements is 2.5 nT. This is an important result in itself, as prior to the mission it was not clear if the lithospheric field could be measured by Ørsted. Although its instrumental accuracy is better than MAGSAT (2.5 nT compared with 4 nT), the higher flight altitude makes detecting higher degrees more difficult.

6. Conclusions

Model Ø19992000_SVM has demonstrated its ability to predict the main magnetic field and its secular variation at the core–mantle boundary for the period 1980–2000. This model can eventually be used to measure the radius of the Earth's core and better define lithospheric field anomalies. In a previous study (Hulot et al., 2002), geomagnetic field variations at the core surface was computed between 1980 and 2000. Strong small-scale geomagnetic field variations were found to be localized below the North Pole and in a region centered below South Africa. In contrast, a large region below the Pacific and the South Pole exhibits weak variations. These features are compared with those obtained from historical, archeomagnetic and paleomagnetic data, as well as with the results of some numerical computations, suggesting that the present day behavior of the geomagnetic field could be

Fig. 6. Amplitude of the crustal field contribution from $N_{\text{i}} = 14$ to 26, in nT, at 740 km, for (a) M102389 (Cain et al., 1989); (b) Ø19992000_SVM; (c) the difference between the two models; (d) the mean altitude of Ørsted measurements.

considered unusual. Another study concerning the dynamics of the core was developed in Langlais (2001), where characteristic times of geomagnetic field from Ø19992000_SVI and Ø19992000_SVM models were estimated. For $N_i \geq 8$, the characteristic times based on Ø19992000_SVI are one order of magnitude higher than those based on Ø19992000_SVM. The combined MAGSAT and Ørsted models will undoubtedly allow new studies of mantle electric conductivity, the coupling between the fluid core and the lower mantle, electric properties of the Earth's outer core, and the relation between length-of-day and geomagnetic processes.

Concerning the crustal field, Mandea and Langlais (2002) estimated the geomagnetic observatory crustal biases using the M19791112 and Ø19991112 models. Computed biases were compared for a set of observatories operating in 1979/1980 (MAGSAT epoch) and 1999/2000 (Ørsted epoch). These comparisons showed their stability over a 20-year time interval. Purucker et al. (2002) compared magnetic field values as predicted by MAGSAT and Ørsted models (for $15 \leq N_i \leq 26$) to those computed from a priori induced and remanent magnetization models over North America. They showed that a priori models can be slightly modified to more closely fit the observations at satellite altitudes, and thus that magnetic data may be used with other geophysical information to better constrain the physical properties of the Earth's lithosphere.

The described Ørsted models do not take into account the ionospheric field. Assuming the ionosphere as a thin, conducting spherical shell, flowing at 110 km mean altitude, its magnetic contribution can be estimated if magnetic measurements are available above and below this 110 km spherical shell (Sabaka and Baldwin, 1993). Furthermore, the ionospheric field has periodic variations (from daily to pluri-annual), which can be determined if the data sampling interval is short enough with respect to the periodic variations to be resolved. In our models, the ionospheric field is considered as a part of the internal contribution, i.e. the Gauss coefficients g_n^m and h_n^m reflect both internal and weak ionospheric fields. Modeling of the ionospheric field will eventually be achieved using satellite and observatory hourly means or even minute values. This would also avoid the need for night local time selection of the satellite data.

Finally, other satellite data sources should not be forgotten. Two more satellites measure the magnetic field, during and after the Ørsted mission. One is the German CHAMP satellite, launched on 15th July 2000, the second is the Argentinean SAC-C satellite, launched on 8th November 2000 These three high-precision magnetic field missions will open opportunities for improving our understanding of the Earth's magnetic field and its internal and external variations.

Acknowledgements

The Ørsted satellite is funded by the Danish Ministry of Transport, the Ministry of Research and Information Technology and the Ministry of Trade and Industry. Additional support was provided by the National Aeronautics and Space Administration, the European Space Agency, Centre National d'Etudes Spatiales and Deutsche Agentur Für Raumfahrtangelegenheiten. Authors wish to thank the many scientists and engineers that contributed to the development, the launch and the ground section of the Ørsted mission, and especially Torsten Neubert, Nils Olsen, Lars Tøffner-Clausen and Kim Bisgaard. All graphs and maps have been plotted using the Generic Mapping Tools software (Wessel and Smith, 1991). This is IPGP contribution no. 1876.

References

Alexandrescu, M., Ha Duyen, C., Le Mouël, J.-L., 1994. Geographical distribution of magnetic observatories and field modelling. J. Geomag. Geoelectr. 46, 891–901.

Backus, G.E., 1968. Applications of a non-linear boundary value problem for Laplace's equation to gravity and geomagnetic intensity surveys. Q. J. Mech. Appl. Math. 12, 195–221.

Barraclough, D.R., 1985. A comparison of satellite and observatory estimates of geomagnetic secular variation. J. Geophys. Res. 90, 2523–2526.

Barraclough, D.R., 1987. International Geomagnetic Reference Field: the fourth generation. Phys. Earth Planet. Inter. 48, 279–293.

Bloxham, J., Jackson, A., 1992. Time-dependent mapping of the magnetic field at the core–mantle boundary. J. Geophys. Res. 97, 19537–19563.

Cain, J.C., Hendricks, S.J., Langel, R.A, Hudson, W.V., 1967. A proposed model for the International Geomagnetic Reference Field—1965. J. Geomag. Geoelectr. 19, 335–355.

Cain, J.C., Frayser, J., Muth, L., Schmitz, D., 1983. The use of MAGSAT data to determine secular variation. J. Geophys. Res. 88, 5903–5910.

Cain, J.C., Wang, Z., Kluth, C., Schmitz, D.R., 1989. Derivation of geomagnetic model to $n = 63$. Geophys. J. 97, 431–441.

Courtillot, V., Le Mouël, J.-L., 1988. Time variations of the Earth's magnetic field: from daily to secular. Ann. Rev. Earth Planet. Sci. 16, 389–476.

Gauss, C.F., 1839. Allgemeine Theorie des Erdmagnetismus, Leipzip.

Hide, R., 1978. How to locate the electrically conducting fluid core of a planet from external magnetic observations. Nature 271, 640–641.

Holme, R., 2000. Modelling of attitude error in vector magnetic data: application to Ørsted data. Earth Planets Space 52, 1187–1197.

Holme, R., Bloxham, J., 1996. The treatment of attitude errors in satellite geomagnetic data. Phys. Earth Planet. Inter. 98, 221–233.

Hulot, G., Eymin, C., Langlais, B., Mandea, M., Olsen, N., 2002. Small-scale structure of the geodynamo inferred from Ørsted and MAGSAT satellite data. Nature 416, 620–623.

Langel, R.A., 1987. The main field. In: Jacobs, J.A. (Ed.), Geomagnetism, vol. 1. Academic Press, London.

Langel, R.A., Estes, R.H., 1985. The near-Earth magnetic field at 1980 determined from MAGSAT data. J. Geophys. Res. 90, 2495–2509.

Langel, R.A, Baldwin, R.T., Green, A.W., 1995. Toward an improved distribution of magnetic observatories for modelling of the main geomagnetic field and its temporal change. J. Geomag. Geoelectr. 47, 475–508.

Langlais, B., 2001, Les champs magnétiques de la Terre et de Mars: apport des satellites Ørsted et Mars Global Surveyor. Ph.D. Thesis (in French). Institut de Physique du Globe de Paris, 306 pp.

Langlais, B., Mandea, M., 2000. An IGRF candidate main geomagnetic field model for epoch 2000 and a secular variation model for 2000–2005. Earth Planets Space 52, 1137–1148.

Langlais, B., Ultré-Guérard, P., Vernin, C., Mandea, M., Cohen, Y., Hulot, G., 1999. Ørsted: IPGP commissioning of the OVH magnetometer. CNES report, OERS-RP-0000-0031-IPG, 28 pp.

Lowes, F.J., 1974. Spatial power spectrum of the main geomagnetic field and extrapolation to the core. Geophys. J. R. Astr. Soc. 36, 717–730.

Malin, S.R.C., Bullard, F.R.S., 1987. The direction of the Earth's magnetic field at London, 1570–1975. Philos. Trans. R. Soc. London 299, 357–423.

Mandea, M., Macmillan, S., 2000. International Geomagnetic Reference Field—the eighth generation. Earth Planets Space 52, 1119–1124.

Mandea, M., Langlais, B., 2002. Observatory crustal magnetic biases during MAGSAT and Ørsted satellite missions. Geophys. Res. Lett. 29, 10.1029/2001GLO13693.

Olsen, N., Holme, R., Hulot, G., Sabaka, T., Neubert, T., Tøffner-Clausen, L., Primdahl, F., Jørgensen, J., Léger, J.M., Barraclough, D., Bloxham, J., Cain, J., Constable, C., Golovkov, V., Jackson, A., Kotzé, P., Langlais, B., Macmillan, S., Mandea, M., Merayo, J., Newitt, L., Purucker, M., Risbo, T., Stampe, M., Thompson, A., Voorhies, C., 2000. Ørsted initial field model. Geophys. Res. Lett. 27, 3607–3610.

Purucker, M., Langlais, B., Olsen, N., Hulot, G., Mandea, M., 2002. The southern edge of cratonic North America: evidence from new satellite magnetometer observations. Geophys. Res. Lett. 10.1029/2001GLO13645.

Sabaka, T.J., Baldwin, R.T., 1993. Modeling the Sq magnetic field from POGO and MAGSAT satellite data and contemporaneous hourly observatory data. Phase1. Contract Rep. HSTX/G&G-9302, Hughes STX Corp. for NASA/GSFC contract NAS5-31760, 100 pp.

Wessel, P., Smith, W.H.F., 1991. Free software helps map and display data. EOS Trans. Am. Geophys. Union 72, 441–448.